Calculation of Mineral Properties with the Electron Gas Model

ROY G. GORDON
Department of Chemistry Harvard University Cambridge, MA 02138

DANIEL J. LACKS†
Department of Chemistry Harvard University Cambridge, MA 02138
† *present address: Department of Chemical Engineering, Tulane University, New Orleans, LA 70118*

Key words. electron-gas model, Density functional theory, silica, phase transitions.

1. Introduction

An understanding of the thermodynamic and mechanical properties of minerals is necessary to explain the structure and dynamics of the earth's interior. Because of the difficulty in determining these properties experimentally at the extreme pressures and temperatures which exist within the earth, computer modeling can yield much information and insight.

The most rigorous methods of calculating the properties of a crystal involve solving the Hartree-Fock or Kohn-Sham equations for the periodic system, and have recently been applied to minerals such as MgO periclase [1, 2], SiO_2 quartz [3], SiO_2 stishovite [4, 5, 6, 7], Mg_2SiO_4 spinel [8, 9], and $MgSiO_3$ perovskite [10, 11]. However the difficulty of these calculations increases rapidly with the size of the unit cell, and for more complex crystals the calculation times prohibit the use of large basis sets and full structure optimizations. Another method of calculating crystal properties uses parameterized force fields, where the parameters are obtained from Hartree-Fock calculations on small molecules or clusters. Such calculations have been carried out for silica and silicates by Tsuneyuki et al. [12] and van Beest et al. [13]. A disadvantage of this method is the ambiguity in determining certain parameters (such as atomic charges) which can vary considerably with the atomic environment [13].

The electron gas model is an alternative, non-empirical, method for the calculation of crystal properties. The electron gas model has the advantages

Molecular Engineering **6**: 63–79, 1996.

that it is more computationally efficient than the periodic Hartree-Fock or Kohn-Sham calculations, and does not have the ambiguity of the force field calculations. In the electron gas model the crystal is assumed to be made up of ions: The total crystal energy is obtained as the interaction energy of the ions in the crystal plus the self-energy of the ions. The self-energies of the ions are obtained by accurate Hartree-Fock or Kohn-Sham methods, and the interaction energy is obtained approximately with density functionals.

The present paper focuses on the application of the electron gas model to the calculation of mineral properties, particularly crystal structures, cohesive energies, electron densities, compressibilities, and pressure-induced phase transitions. The effects of partial covalent bonding, or equivalently the non-spherical distortions of the ions, on these properties are addressed.

2. Computational Method

2.1. THEORY

The electron gas model is characterized by three assumptions [14]:

1. The interaction energy DE is calculated with energy functionals of the electron density,

$$\Delta E = \int \left\{ \epsilon[\rho(\mathbf{r})] - \sum_i \epsilon[\rho_i(\mathbf{r} - \mathbf{r_{oi}})] \right\} \tag{1}$$

where ϵ is the density functional, ρ is the electron density of the total system, ρ_i is the electron density of the ion centered at $\mathbf{r_{oi}}$, and the sum is over the interacting ions in the system. This calculation of the interaction energy would be exact if the exact density functional was known; however, only approximate density functionals are known.

2. The total electron density $\rho(\mathbf{r})$ is the sum of the electron densities of the ions ρ_i in the system:

$$\rho(\mathbf{r}) = \sum_i \rho_i(\mathbf{r} - \mathbf{r_{oi}}) \tag{2}$$

This additive density approximation does not correspond to the antisymmetrized product of the ionic wavefunctions which give the densities ρ_i; however, the resulting electron density does correspond to some antisymmetrized (although unknown) wavefunction, and thus does not violate the Pauli exclusion principle [15]. If there were full variability in the ρ_i, any total electron density ρ could be constructued and the additive density approximation would not limit the accuracy of the calculation. In practice, however, the limited variability in the ionic densities restricts the possibilities for the total electron density and thus the accuracy of the calculation.

3. The electron densities of the ions, ρ_i, are obtained from accurate quantum mechanical calculations, such as Hartree-Fock or Kohn-Sham calculations, on the isolated ions. Changes in the ionic densities ρ_i due to the crystal environment can be incorporated by including a perturbative potential in the ionic calculation. The self-energy of the ion is calculated as the energy of the ion with the perturbed density (the energy does not include the perturbation energy) minus the energy of the gas phase, stable ion (For oxides, since O^{2-} is unstable in the gas phase, the reference ion is O^-).

2.2. APPROXIMATIONS

The electron gas model would give exact results if an exact density functional were used for the interaction energy, the ionic densities were fully variable so that any total density could be obtained by summing the ionic densities, and the calculation of the ionic self-energies were exact. In practice these conditions cannot be met and approximations must be used.

2.2.1. *Density functionals for interaction energy*

The exact density functionals for arbitrary electron densities are not known. The simplest approximate density functionals are those which are exact for the uniform electron gas [16, 17] (the correlation energy functional is known exactly for the uniform electron gas only in the limits of high and low electron densities; the correlation energy for intermediate densities can be obtained by interpolation between these limits [14]). To improve upon the uniform electron gas functionals, Waldman and Gordon introduced scaling coefficients which depend on the number of electrons in the system [18]. Although these scaled functionals increase the accuracy of electron gas model calculations, this increased accuracy is due somewhat to a cancellation of the error due to the approximate electron density [19]. Accurate non-local density functionals have recently been developed [20, 21, 22], which lead to more accurate calculations of interaction energies [19, 22].

2.2.2. *Electron densities*

In the simplest formulations of the electron gas model, gas phase ionic densities are used for the crystalline ionic electron densities [23]. However, to increase the accuracy of the model, changes in the ionic densities in response to the crystalline environment must be incorporated. The changes in ionic density are non-spherical in general, although a spherical ion approximation is valid when the ion is in a high symmetry position. Most of the earlier electron gas model calculations assumed spherical ions for simplicity; more recent work has been directed towards non-spherical distortions.

The changes in the ionic electron densities have been incorporated in three ways:

1. An electrostatic perturbation is included in the ionic calculation, the parameters of which are chosen to reproduce the electrostatic environment of the ion in the crystal. The electrostatic perturbation is a charged spherical shell for spherical ion calculations [24, 25], and a series of point charges for non-spherical ion calculations [26].
2. An electrostatic perturbation is included in the ionic calculation, the parameters of which are varied to minimize the total crystalline energy. By varying the parameters to minimize the total crystal energy, rather than to reproduce the electrostatic environment of the ion in the crystal, all factors which affect the electron density – including short range repulsions caused by overlap of the ionic densities – are taken into account, rather than just the electrostatic factors. These variational calculations have been carried out both for spherical [27] and non-spherical ions [28].
3. The effects of the other ions in the crystal are included directly in the Hamiltonian for the electronic structure calculation for the ion; the electron densities of the ions are obtained self-consistently as those which minimize the total crystalline energy. This method, which corresponds to the variational electrostatic perturbation method with an infinite number of variational parameters, has been applied in both the spherical ion approximation [29, 30] and the general non-spherical case [31].

In practice, since the cation electrons are more tightly bound than the anion electrons, the changes in the cation densities are small compared to the changes in the anion densities and are generally neglected [24].

2.2.3. *Ionic self energies*

When the Hartree-Fock method is used for the ionic calculation, the error due to the neglect of electron correlation is significant if the number of electrons in the crystal ion is different from that in the reference gas phase ion (this occurs for oxides, where the crystal ion is O^{2-} and the reference gas phase ion is O^{-}). Earlier electron gas calculations estimated the self-energy due to electron correlation [24], but in more recent calculations an accurate non-local correlation energy functional [32] was used to evaluate this part of the self-energy [28].

The basis set superposition error must also be accounted for when small basis sets are used (small basis sets are used in the distorted ion calculations [28, 31]; the basis sets are large enough so that this effect is neglible in the spherical ion calculations). A counterpoise method, in which the energy of

the gas phase ion is calculated with a basis set similar to that used in the crystal calculation, is used to minimize this error [28].

3. Spherical ion calculations of mineral properties

Many calculations of mineral properties have been carried out with spherical ion electron gas models. For example, early investigations of CaO predicted that the B1 phase would transform to the B2 phase at approximately 1 megabar [33]; later experiments substantiated this prediction [34]. Results for silica predicted that stishovite would transform to the $CaCl_2$ structure at megabar pressures [35]; subsequent experimental evidence suggested that this phase transition does in fact occur at approximately 1 megabar [36, 37]. Temperature and pressure dependences of the structural and elastic properties of simple oxide minerals have also been calculated [27, 38, 39, 40].

The spherical ion models, however, give poor results for crystals in which the anions occupy low symmetry positions, such as the silica polymorphs quartz and cristobalite, the silicate diopside, and the zeolite sodalite [41, 42, 43]. The non-spherical distortions are expected to be significant for anions in low symmetry positions; For example, in the quartz structure the oxygen anion has two neighboring silicon cations at an angle of 143° and the oxygen electron density is significantly distorted towards the silicon cations [44]. To obtain meaningful results for such crystals, non-spherical distortions of the ionic electron densities must be incorporated.

4. Distorted ion calculations of mineral properties

The results discussed below were obtained with a variational electrostatic perturbation for calculating the anion electron densities, and the scaled density functionals for calculating the interaction energies. These results have been presented in more detail elsewhere [28, 45, 46].

4.1. STRUCTURES AND COHESIVE ENERGIES

Results for structural parameters and the cohesive energies of several partially covalent crystals are given in Table 1 (For the open structures, the most sensitive structural parameter is the cation-anion-cation bond angle; for close-packed systems, these angles are constrained by the packing, and the cation-anion bond length is the most sensitive parameter). For systems with open crystal structures, the structures and energies calculated with distorted ions are in much better agreement with experiment than those calculated with spherical ions. The improved structural results are due to smaller and more accurate cation- anion-cation bond angles, and the improved energetic results are due to the stronger bonds formed when charge

density moves into the bonding regions. For systems with close- packed structures, the structures are modeled well with both the distorted and spherical ion models, but the energies are calculated more accurately with the distorted ions.

TABLE 1.
Structural Results. Calculated results are from reference 28; experimental results are quoted from reference 28.

Open Structures	Cation-Anion-Cation Angle (°)			Cohesive Energy (kJ/mol)		
	exper.	distorted	spherical	exper.	distorted	spherical
SiO_2 Quartz	142	143	163	-11530	-11470	-11080
SiO_2 Cristobalite	145	150	180	-11530	-11470	-11110
$Na_4ClSi_3Al_3O_{12}$ Sodalite	138	137	156	–	-57550	-56160
BeF_2 Quartz	–	145	161	–	-3730	-3390
Close-Packed Structures	Cation-Anion-Cation Angle (°)			Cohesive Energy (kJ/mol)		
	exper.	distorted	spherical	exper.	distorted	spherical
SiO_2 Stishovite	1.81[a]	1.77	1.75	-11470	-11450r	-10880
	1.76[b]	1.76	1.74			
Mg_2SiO_4 spinel	1.66[c]	1.67	1.60	-17620	-17670	-17040
	2.07[d]	2.01	2.08			
$MgSiO_3$ perovskite	1.79[c]	1.73	1.74	–	-14440	-13970
TiO_2 Rutile	1.98[a]1.95	1.91	-10400	-10080	-9910	
	1.94[b]	1.96	1.94			

[a] 1 bond per oxygen ion

[b] 2 bonds per oxygen ion

[c] Si-O bond

[b] Mg-O bond

4.2. ELECTRON DISTRIBUTIONS

The valence electron density distributions of cristobalite, stishovite, spinel and perovskite are shown in Figure 1 (the electron distribution of quartz, which is not shown, is essentially identical to that of cristobalite). The non-spherical distortions are significant, and agree well with the results of crystalline Hartree-Fock calculations [47]. In general, there are approximately 0.3-0.5 electrons in the bonding regions, by Mulliken population analysis.

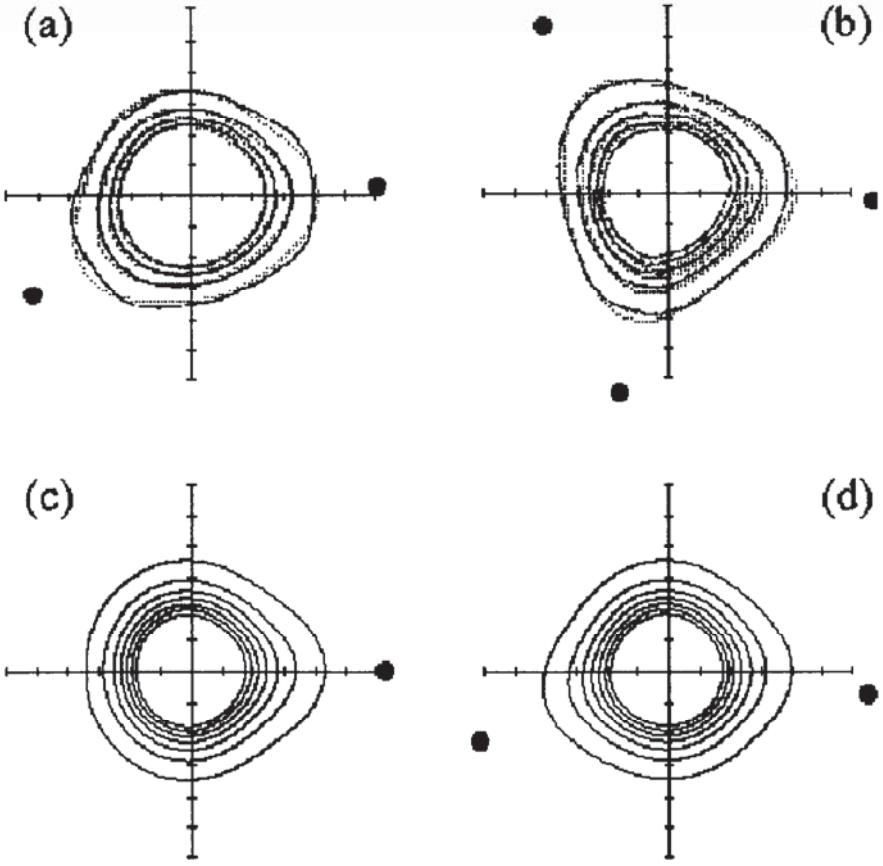

Fig. 1. Valence electron distributions, in the plane of the oxygen anion and the neighboring cations. The oxygen anion is centered at the origin, and the filled circles are the positions of the neighboring silicon cations. Contour lines are spaced at 0.5 electrons/Å^3, and the length of the axes are 1.588 Å.
(a) Cristobalite, (b) Stishovite. Solid lines: crystalline Hartree-Fock calculation ; Dotted lines: Electron gas model.
(c) Spinel, (d) Perovskite. Solid lines: Electron gas model.

The non-spherical distortions are as large in the close-packed stishovite structure as in the open cristobalite structure; therefore, stishovite is not significantly more ionic than cristobalite (or quartz). However, the distortions are smaller in the perovskite structure than in the cristobalite, stishovite or spinel structures, and so the bonding in perovskite can be considered more ionic than in these other structures.

The oxygen electron density in spinel is found to be polarized much more towards the silicon ion than towards the magnesium ions (the three neigboring magnesium ions are in the direction opposite to the silicon ion).

This result occurs because the extent of polarization is proportional to the electric field at the anion, and the electric field from a silicon ion (with a charge of +4 and at a distance of 1.66) is significantly greater that from a magnesium ion (with a charge of +2 and at a distance of 2.07).

4.3. STRUCTURAL CHANGES AT HIGH PRESSURES

As discussed above, whereas for open structures the zero-pressure structures are calculated more accurately with the distorted ion model than with the spherical ion model, for close-packed systems the zero-pressure structures are calculated just as well with the spherical ion model. In the same way, the distorted ion model leads to improvements in the compression at high pressures for open structures but not for close-packed structures. Although the agreement with experiment is reasonable for calculated changes in volume with pressure, the calculated structures are generally less compressible than observed experimentally (i.e., the bulk moduli are too high).

For example, Figure 2 shows the change in volume with pressure for quartz. The large compressibility is reproduced well with the distorted ion model, but poorly with the spherical ion model, because the change in volume is due primarily to the decrease in the Si-O-Si angle (the bond length varies only slightly) [48, 49, 50]. The bulk modulus, K, and its pressure derivative, K', for quartz are K=47 GPa and K'=7.9 with the distorted ion model, K=229 GPa and K'=7.5 with the spherical ion model, and K=34-37 GPa and K'=5.7-6.2 experimentally [49, 50]. Therefore, the distorted ion model greatly improves the bulk modulus relative to the spherical ion model, but still overestimates the bulk modulus somewhat.

4.4. PRESSURE-INDUCED PHASE TRANSITIONS

4.4.1. *Quartz to stishovite phase transition*

As the pressure is increased, silica undergoes a phase transition from quartz to coesite at 3 GPa, which in turn transforms to stishovite at 8 GPa (for temperatures of 1000 K) [51]. Stishovite differs from quartz and coesite in that the silicon ions are coordinated to six oxygen ions in stishovite, as compared to only four oxygen ions in quartz and coesite. This increase in the coordination of the silicon ion allows a much denser structure, with an associated volume decrease of about 38% [52]. Although the equilibrium transformation of quartz to stishovite proceeds through the coesite intermediate phase, the coesite phase is ignored in the present calculations for simplicity.

The calculated enthalpies for silica in the quartz and stishovite phases are shown in Figure 3 as a function of pressure. The stishovite structure becomes more stable than the quartz structure at 3.5 GPa with the dis-

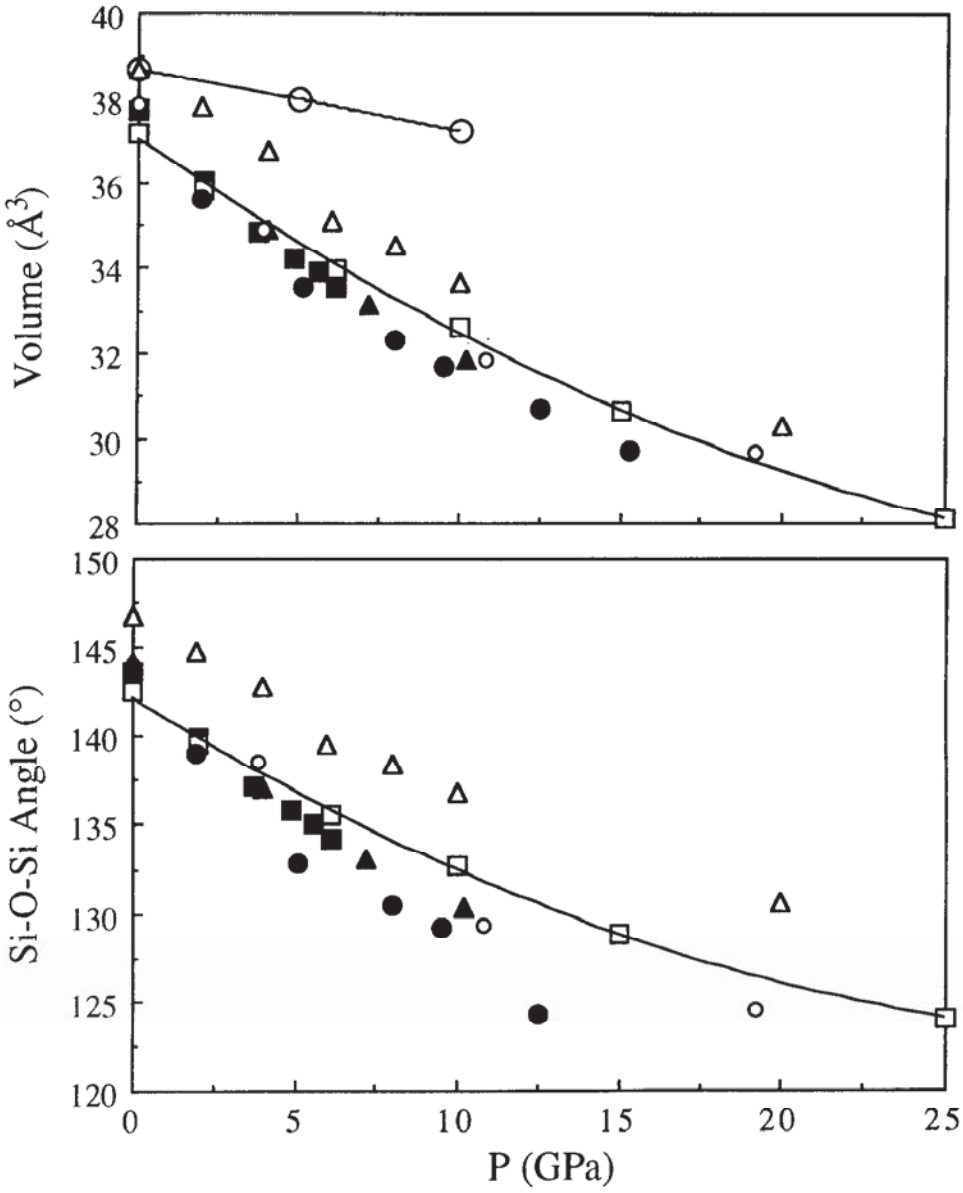

Fig. 2. α-Quartz structure as a function of pressure. Open squares: distorted ion electron gas model; open large circles: spherical ion electron gas model; open triangles: TTAM model; open small circles: pseudopotential plane wave calculations of Chelikowsky et al. [3]; filled triangles: experimental results of Glinneman et al. [48]; filled squares: experimental results of Levien et al. [49]; filled circles: experimental results of Hazen et al. [50]. The spherical ion electron gas model Si-O-Si angles are all greater than 160 degrees.

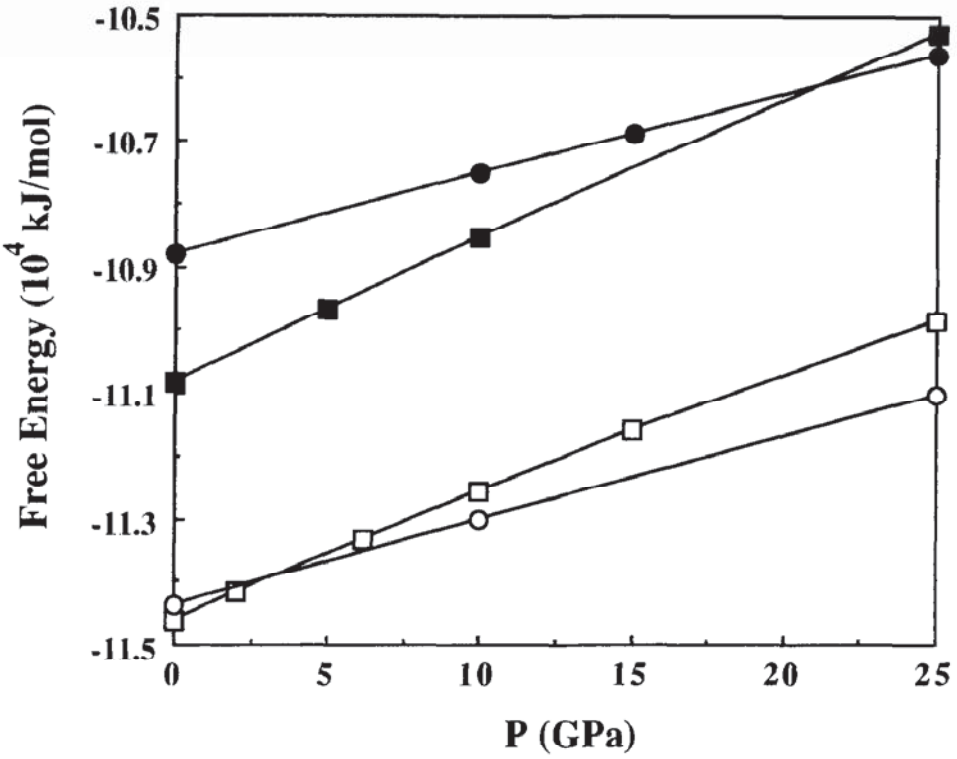

Fig. 3. Enthalpy of silica in quartz and stishovite structures as a function of pressure. Key: squares: quartz, circles: stishovite; open symbols: distorted ion electron gas model, closed symbols: spherical ion electron gas model.

torted ion model, and at 21 GPa with the spherical ion model. In comparison, the experimental zero temperature transition pressure for the quartz to stishovite phase transition is estimated to be 5.5 GPa from thermodynamic data [53], and the transition pressure for the similar cristobalite to stishovite phase transition is calculated to be 6 GPa by periodic Hartree-Fock methods [54]. The non-spherical distortions improve the modeling of this phase transition by stabilizing stishovite with respect to quartz; the greater stabilization of stishovite occurs because the distortions strengthen three bonds per anion in stishovite, and only two bonds per anion in quartz (the bonds are significantly covalent in both structures, as shown above in the plots of the electron density distributions).

4.4.2. *Stishovite to $CaCl_2$-type structure phase transition*

Upon further compression, stishovite is believed to undergo further phase transitions, although these are not well understood. Analogous systems showed transitions from the stishovite-type (rutile) structure to the $CaCl_2$-type structure [55], which is a slight distortion of the stishovite structure; the stishovite structure is a special case of the $CaCl_2$ structure in which the lattice parameters a and b, and the oxygen position parameters x and y, are equal. Spherical ion electron-gas calculations first predicted that stishovite would transform to the $CaCl_2$ structure at megabar pressures [35], and evidence from subsequent experiments suggest that this phase transition occurs at approximately 100 GPa [36, 37].

The changes in the lattice parameters and the oxygen position parameters with pressure are shown in Figure 4. The distorted ion model predicts the phase transition to occur at slightly under 200 GPa, and although not shown, the spherical ion model predicts the phase transition to occur at 500 GPa. The distortion of the oxygen ions decreases the calculated transition pressure considerably, due to the interaction of the dipoles that form when the distorted anion moves out of the plane of the silicon ions. We note that the transition pressure with the distorted ion model is still somewhat larger than the pressure suggested by experiment [36, 37], and the pressures of 45 to 80 GPa obtained in periodic electronic structure calculations [4, 5].

4.4.3. *Spinel to perovskite phase transitions in $MgSiO_3$ and Mg_2SiO_4*

The seismic discontinuity occuring in the earth's mantle at a depth of 670 km is attributed to the phase transition from the spinel phase to the perovskite phase, and it is this discontinuity which marks the separation between the upper and lower mantle. Calculations were carried out of this phase transition in the $MgSiO_3$ and Mg_2SiO_4 systems, which approximately model the composition of the mantle.

The results of the distorted ion calculations for the enthalpies relevant to this phase transition are shown in Figure 5a. At zero pressure, spinel is the most stable phase. At 24.5 GPa, the two-oxide assemblage (MgO periclase + SiO_2 stishovite) becomes stable, and remains stable to 31.5 GPa, at which point the perovskite phase becomes stable. The spinel to perovskite phase transition occurs at 26.0 GPa for the Mg_2SiO_4 stoichiometry, and at 27.0 GPa for the $MgSiO_3$ stoichiometry. These results are in good agreement with extrapolations to zero temperature of experimental results, which find the spinel to perovskite phase transition to occur at 27.4 GPa for the Mg_2SiO_4 stoichiometry and at 27.7 GPa for the $MgSiO_3$ stoichiometry, and also that the two-oxide assemblage is the most stable form in the pressure range 26.7 GPa to 28.0 GPa [56]. In contrast, the spherical ion results, shown in Figure 5b, are in poor agreement with the experi-

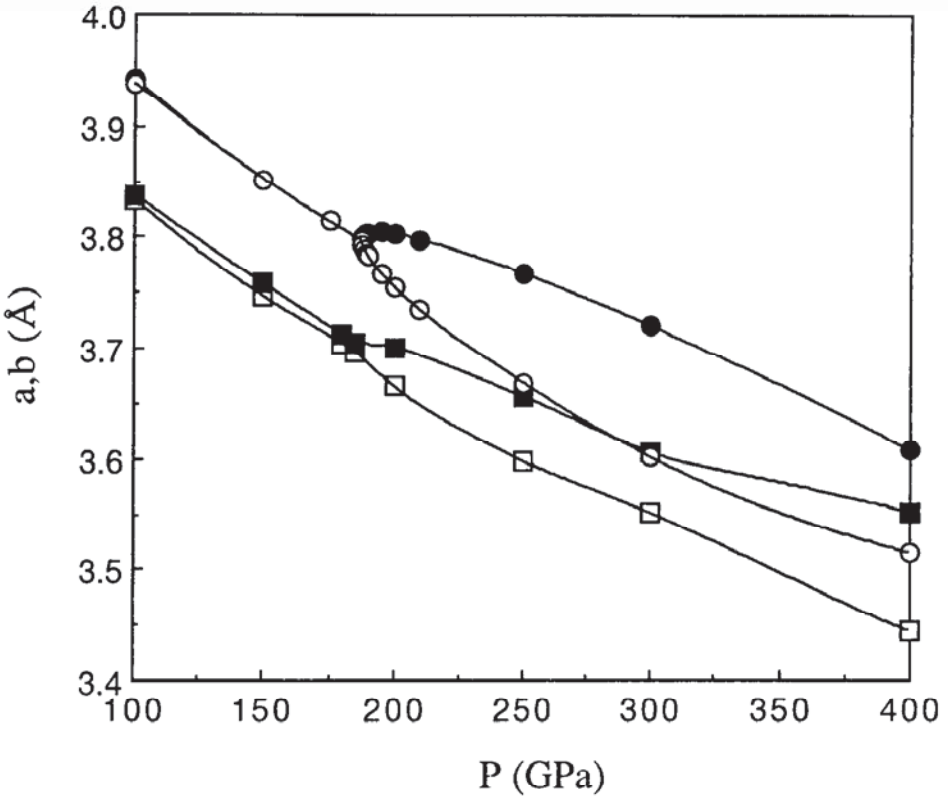

Fig. 4. $CaCl_2$ a, b lattice parameters as a function of pressure. When $a = b$, the $CaCl_2$ structure reduces to stishovite. Squares: distorted ion electron gas model; circles: TTAM model.

mental extrapolations. The inclusion of covalent bonding effects improves the results by stabilizing the spinel and stishovite structures relative to the perovskite and periclase structures – the anions were shown above to be significantly more distorted in spinel and stishovite than in perovskite.

5. Conclusions

The inclusion of non-spherical distortions of the ions, or equivalently covalent bonding effects, in the electron gas model leads to improved results for the properties of minerals. For crystals which have open structures, the structures, energies and compressibilities calculated with the distorted ion model are in much better agreement with experiment than those calculated with spherical ion model; the improved structures are due mainly to smaller and more accurate cation-anion-cation bond angles and the improved en-

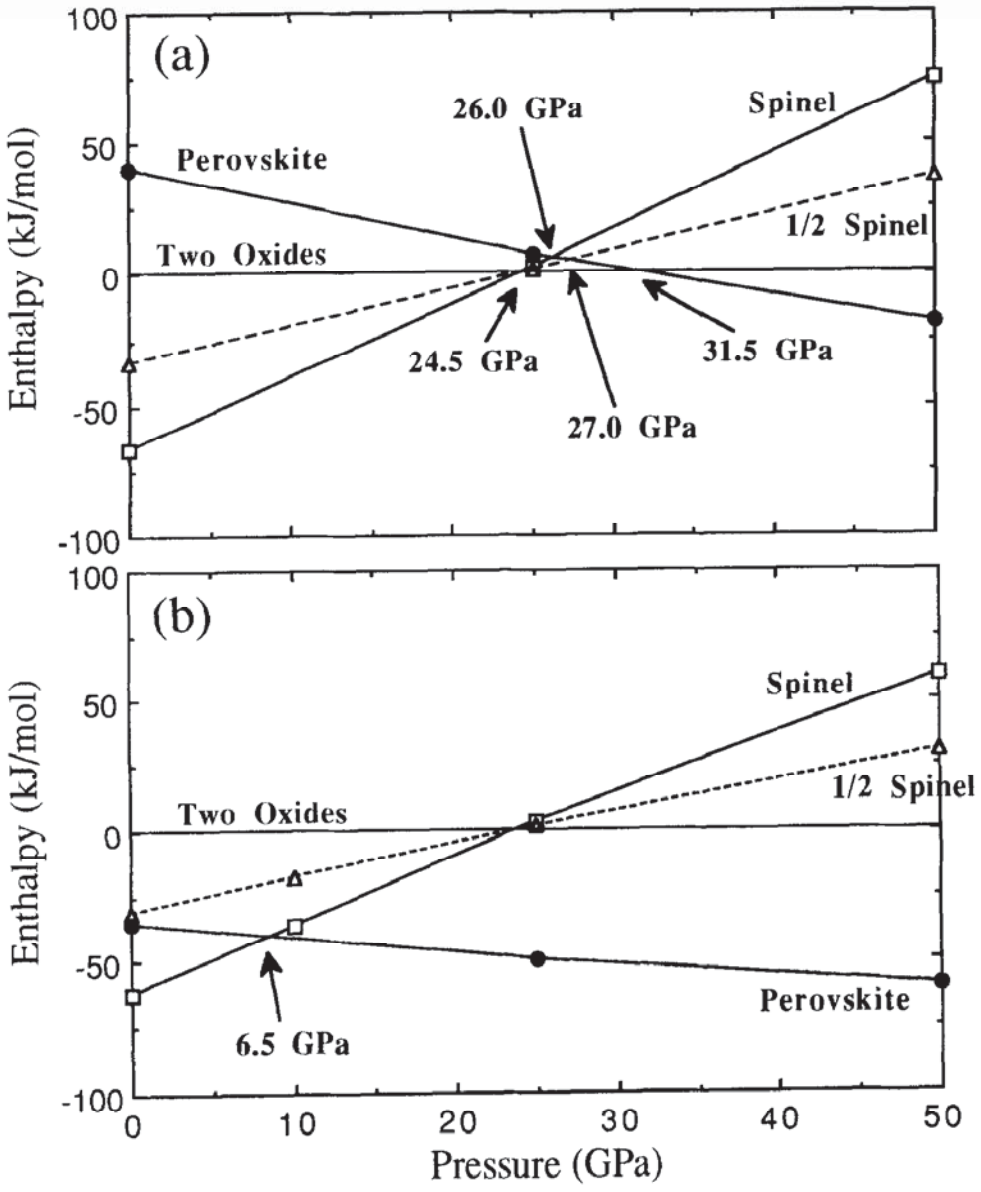

Fig. 5. Enthalpies of phases in Magnesium Silicate system as a function of pressure, relative to the binary oxides (stishovite and periclase). (a) distorted ion electron gas model; (b) spherical ion electron gas model.

ergies are due to the stronger bonds formed when charge density moves into the bonding regions. For crystals which have close-packed structures, the structures and compressibilites are modeled well with the spherical ion model, but the energies are calculated more accurately with the distorted ion model. The distorted ion model leads to improved modeling of pressure-induced phase transitions, due to the more accurate calculation of the crystal structures, compressibilities and energies.

The effects of covalency on the quartz to stishovite phase transition in silica and the spinel to perovskite phase transition in magnesium silicates can be compared. Both of these phase transitions are from a phase based on tetra-coordinated silicon ions to a phase based on hexa-coordinated silicon ions. For the phase transition in silica, the inclusion of covalent effects reduces the transition pressure by over 15 GPa: stishovite is stabilized relative to quartz because it has more bonds, and the bonds are significantly covalent in both structures. In contrast, for the magnesium silicate phase transition, the inclusion of covalent effects increases the transition pressure by 20 GPa: although there are more bonds in perovskite than in spinel, spinel is stabilized more because the bonds are more covalent in spinel than in perovskite.

Acknowledgements

We thank Dr. Harry Hummel for many valuable discussions and the use of his program for the spherical ion calculations, and Dr. Bernard Silvi for plotting the electron density curves from his crystalline Hartree-Fock calculations. This work was supported in part by the National Science Foundation and the National Renewable Energy Laboratory.

References

1. Bukowinski, M.S.T. (1985) First principles equations of state of MgO and CaO, *Geophys. Res. Lett.* **12**,536-539.
2. Mehl, M.J., Cohen, R.E. and Krakauer, H. (1988) Linearized augmented plane wave electronic structure calculations for MgO and CaO *J. Geophys. Res.* **93**, 8009-8022.
3. Chelikowsky, J.R., King, H.E., Troullier, B., Martins, J.L. and Glinnemann, J. (1990) Structural properties of α-quartz near the amorphous transition *Phys. Rev. Lett.* **65**,3309-3312.
4. (a) Cohen, R.E. (1991) Bonding and elasticity of stishovite SiO_2 at high pressure: linearized augmented plane wave calculations *Am. Miner.* **76**, 733-742.; (b) Cohen, R.E. (1992) First principles predictions of elasticity and phase transitions in high pressure SiO_2 and geophysical applications, in Y. Syono and M.H. Manghnani (eds.), *High-Pressure Research: Application to Earth and Planetary Sciences,* Terra Scientific, Tokyo, pp 425-431.
5. (a) Jolly, L-H., Silvi, B.and D'Arco Ph. (1994) Periodic Hartree-Fock study of minerals: Hexacoordinated SiO_2 and GeO2 polymorphs *Eur. J. Mineral.* **6**, 7-16.; (b) Jolly, L-H., Silvi, B. and D'Arco Ph. (1993) Periodic Hartree-Fock investigation of

the stishovite $CaCl_2$-like phase transition of silica *J. Chim. Phys.* **90**,1887-1895.
6. Keskar, N., Troullier, N., Martins, J.L. and Chelikowsky, J.R. (1991) Structural properties of SiO_2 in the stishovite structure *Phys. Rev.* **B44**, 4081-4088.
7. Sherman, D.M. (1993) Equation of state and high-pressure phase transitions of stishovite (SiO_2): ab initio (periodic hartree-fock) results *J. Geophys. Res.* **98**, 11865-11873.
8. D'Arco, Ph., Silvi, B., Roetti, C. and Orlando, R. (1991) Comparative study of spinel compounds: a pseudopotential periodic Hartree-Fock calculation of Mg_2SiO_4, Mg_2GeO4, Al2MgO4 and Ga2MgO4 *J. Geophys. Res.* **96**,6107-6112.
9. Silvi, B., Bouaziz, A., and D'Arco Ph., Pseudopotential periodic Hartree-Fock study of Mg_2SiO_4 polymorphs: olivine, modified spinel and spinel *Phys. Chem. Minerals* **20**,333-340.
10. Wentzcovitch, R.M., Martins, J.L. and Price, G.D. (1993) Ab initio molecular dynamics with variable cell shape: application to $MgSiO_3$ *Phys. Rev. Lett.* **70**, 3947-3950.
11. D'Arco, Ph., Sandrone, G., Dovesi, R., Orlando, R. and Saunders, V.R. (1993) A Quantum mechanical study of the perovskite structure type of $MgSiO_3$ *Phys. Chem. Minerals* **20**, 407-414.
12. Tsuneyuki, S., Tsukada, M., Aoki, H. and Matsui, Y. (1988) First principles interatomic potentials of silica applied to molecular dynamics *Phys. Rev. Lett.* **61**,869-872.; Tsuneyuki, S., Matsui, Y., Aoki, H. and Tsukada, M. (1989) New pressure induced structural transformations in silica obtained by computer simulation *Nature* **339**, 209-211.
13. van Beest, B.W.H., Kramer, G.J. and van Santen, R.A. (1990) Force fields for silica and aluminophosphates based on ab initio calculation *Phys. Rev. Lett.* **64**, 1955-1958.
14. Gordon, R.G. and Kim, Y.S. (1972) Theory for the forces between closed shell atoms and molecules *J. Chem. Phys.* **56**, 3122-3133.
15. Gilbert, T.L. (1975) Hohenberg-Kohn theorem for nonlocal external potentials *Phys. Rev.* **B12**, 2111-2120.
16. Thomas, L.H. (1927) The calculation of atomic fields *Proc. Camb. Phil. Soc.* **23**,542-548.; Fermi, E. (1927) Un metodo statistice per la determinazione di alcune proprieta dell'atomao *Rend. Accad. Lincei* **6**, 602-607.
17. Dirac, P.A.M. (1930) Note on exchange phenomena in the Thomas atom, *Proc. Camb. Phil. Soc.* **26**, 376-385.
18. Waldman, M. and Gordon, R.G. (1979) Scaled electron gas approximation for intermolecular forces *J. Chem. Phys.* **71**,1325-1329.
19. Lacks, D.J. and Gordon, R.G. (1994) Tests of non-local kinetic energy functionals *J. Chem. Phys.* **100**, 4446-4452.
20. 20. Perdew, J.P., Yue, W. (1986) Accurate and simple density functional for the electronic exchange energy: Generalized gradient approximation *Phys. Rev.* **B33**, 8800-8802.
21. Lee, H., Lee, C. and Parr, R.G. (1991) Conjoint gradient correction to the Hartree-Fock kinetic- and exchange-energy density functionals *Phys. Rev.* **A44**, 768-771.
22. Lacks, D.J. and Gordon, R.G. (1993) Pair Interactions of Rare Gas Atoms as a Test of Exchange Energy Density Functionals in Regions of Large Density Gradients *Phys. Rev.* **A47**, 4681-4691.
23. Kim, Y.S. and Gordon, R.G. (1974) Theory of binding in ionic crystals: Application to alkali-halide and alkaline-earth dihalide crystals *Phys. Rev.* **B9**, 3548-3554.
24. Muhlhausen, C. and Gordon, R.G. (1981) Electron gas theory of ionic crystals, including many-body effects *Phys. Rev.* **B23**, 900-923; Muhlhausen, C. and Gordon, R.G. (1981) Density-functional theory for the energy of crystals: test of the ionic model *Phys. Rev.* **B24**, 2147-2160.
25. Boyer, L.L., Mehl, M.J., Feldman, J.L., Hardy, J.R., Flocken, J.W., Fong, C.Y. (1985) Beyond the rigid-ion approximation with spherically symmetric ions *Phys.*

Rev. Lett. **54,** 1940-1943.
26. LeSar, R. and Gordon, R.G. (1982) Electron gas model for molecular crystals. Application to the alkali and alkaline earth hydroxides *Phys. Rev.* **B25,** 7221-7237.
27. Wolf, G.H. and Bukowinski, M.S.T. (1988) Variational stabilization of the ionic charge densities in the electron-gas theory of crystals: applications to MgO and CaO *Phys. Chem. Minerals,* **15,** 209 -220.
28. Lacks, D.J. and Gordon, R.G. (1993) Crystal structure calculations with distorted ions *Phys. Rev.* **B48,** 2889-2908.
29. LeSar, R. (1983) Ground- and excited-state properties of solid argon under pressure *Phys. Rev.* **B28,** 6812-6820; LeSar, R. (1988) Equation of state of dense helium *Phys. Rev. Lett.* **61,** 2121-2124.
30. Zhang, H. and Bukowinski, M.S.T. (1991) Modified potential-induced-breathing model of potentials between closed shell ions *Phys. Rev.* **B44,** 2495-2503.
31. Hummel, H.H (1993) Density functional theory of ionic solids: theory and application, Ph.D. Thesis, Harvard University.
32. Perdew, J.P., Cevary, J.A., Vosko, S.H., Jackson, K.A., Pederson, M.R., Singh, D.J., and Fiolhais, C. (1992) Atoms, molecules, solids and surfaces: applications of the generalized gradient approximation for exchange and correlation *Phys. Rev.* **B46,** 6671-6687.
33. Cohen, A.J. and Gordon, R.G. (1976) Modified electron-gas study of the stability, elastic properties, and high-pressure behavior of MgO and CaO crystals*Phys. Rev.* **B14,** 4593-4605.
34. Jeanloz, R., Ahrens, T.J., Mao, H.K., Bell, P.M. (1979) B1-B2 transition in calcium oxide from shock-wave and diamond-anvil experiments *Science* **206,** 829-830.
35. Hemley, R.J., Jackson, M.D. and Gordon, R.G. (1985) Lattice dynamics and equations of state of high-pressure mineral phases studied with electron gas theory *EOS Trans. AGU* **66,** 357.
36. 36.Hemley, R.J. (1987) Pressure dependence of Raman spectra of SiO_2 polymorphs: α-quartz, coesite, and stishovite, in M. H. Manghnani and Y. Syono (eds.), *High-Pressure Research in Mineral Physics,* American Geophysical Union, Washington, pp. 347-359.
37. Tsuchida, Y. and Yagi, T. (1989) A new, post stishovite high pressure polymorph of silica *Nature* **340,** 217-220.
38. Hemley, R.J., Jackson, M.D. and Gordon, R.G. (1985) First-principles theory for the equations of state of minerals at high pressures and temperatures: Application to MgO *Geophys. Res. Lett.* **12,** 247-250.
39. Cohen, R.E. (1987) Calculation of elasticity and high pressure instabilities in corundum and stishovite with the potential induced breathing model *Geophys. Res. Lett.* **14,** 37-40.
40. Isaak, D.G., Cohen, R.E. and Mehl, M.J. (1990) Calculated elastic and thermal properties of MgO at high pressures and temperatures *J. Geophys. Res.* **95,** 7055-7067.
41. Post, J.E. and Burnham, C.W. (1986) Ionic modeling of mineral structures and energies in the electron gas approximation: TiO2 polymorphs, quartz, forsterite, diopside *Am. Miner.,* **71,** 142-150.
42. Jackson, M.D. and Gordon, R.G. (1988) MEG investigation of low-pressure silica: Shell model for polarization *Phys. Chem. Minerals* **16,** 212-220.
43. Hummel, H.H. and Gordon, R.G. (1989) in J. Tersoff, D. Vanderbilt and V. Vitek (eds.), *Atomic Scale Calculations in Materials Science,* M.R.S Symposia Proceedings No. 141, Materials Research Society, Pittsburgh (1989).
44. Stewart, R.F. and Spackman, M.A. (1981) Charge density distributions, in M. O'Keefe and A. Navrotsky (eds.), *Structure and Bonding in Crystals, Vol II.,* Academic Press, Orlando, pp. 279-278.
45. Lacks, D.J. and Gordon, R.G. (1993) Calculations of pressure induced phase transitions in silica *J. Geophys. Res.* **98,** 22147-22155.

46. Lacks, D.J. and Gordon, R.G. (1994) Calculations of pressure induced phase transitions in mantle minerals *Phys. Chem. Minerals,* submitted.
47. Silvi, B. (1992) personal communication; Silvi, B., Allavena, M., Hannachi, Y. and D'Arco, Ph. (1992) Pseudopotential periodic Hartree-Fock study of the cristobalite phases of silica and germanium dioxide, J. Amer. Ceram. Soc. **75,** 1239-1246.
48. Glinneman, J., King, H.E., Schulz, H., Hahn T., LaPlaca, S.J. and Dacol F. (1992) Crystal structures of the low-temperature quartz-type phases of SiO_2 and GeO2 at elevated pressure *Z. Krist.* **198,** 177-212.
49. Levien, L., Prewitt, C.T. and Weidner, D.J. (1980) Structure and elastic properties of quartz at pressure *Am. Miner.* **65,** 920-930.
50. Hazen, R.M., Finger LW, Hemley, R.J. and Mao, H.K. (1989) High pressure crystal chemistry and amorphization of α-quartz *Solid State Comm.* **72,**507-511.
51. Akimoto, S., Yagi, T. and Inoue, K. (1977) High temperature-pressure phase boundaries in silicate systems using in situ x-ray diffraction, in M. H. Manghnani and S. Akimoto (eds.), *In High-pressure Research: Applications to Geophysics,* Academic Press, New York, pp. 585-602.
52. Jamieson, J.C., Manghnani, M.H. and Ming, L.C. (1981) Crystal chemical effects on geophysical equilibrium, in M. O'Keefe and A. Navrotsky (eds.), *Structure and Bonding in Crystals, Vol II.,* Academic Press, Orlando, pp. 95-106.
53. Robie, R.A., Hemingway, B.S., and Fisher, J.R. (1979) Thermodynamic properties of minerals and related substances at 298.15 K and 1 bar (105 pascals) pressure and at higher temperatures, p. 21, Geological Survey Bulletin 1452.
54. Silvi, B., Jolly, L-H. and D'Arco, Ph. (1992) Pseudopotential periodic Hartree-Fock study of the cristobalite to stishovite phase transition *J. Mol. Struct.* **260,** 1-9.
55. Worlton, T.G. and Beyerlein, R.A. (1975) Structure and order parameters in the pressure induced continuous transition in TiO2 *Phys. Rev.* **B12,** 1899-1907.
56. Gasparik, T. (1992) Melting experiments on the enstatite-pyrope join at 80-152 kbar *J. Geophys. Res.* **97,** 15181-15188.